Configuring and Verifying Reverberation Chambers for Testing Cellular Wireless Devices

Kate A. Remley, *Fellow, IEEE*, Jos Dortmans, *Student Member, IEEE*, Catherine Weldon, Robert D. Horansky, *Member, IEEE*, Thomas B. Meurs, *Student Member, IEEE*, Chih-Ming Wang, Dylan F. Williams, *Fellow, IEEE*, Christopher L. Holloway, *Fellow, IEEE*, and Perry F. Wilson, *Fellow, IEEE*

***Abstract*—Reverberation chambers provide a repeatable test environment for laboratory over-the-air testing and represent a viable solution for testing large-form-factor wireless devices. Such tests often involve "imperfect chamber" configurations in which the chamber is loaded with RF absorbing material. We provide step-by-step guidance on configuring and verifying chamber performance for over-the-air tests of single-antenna cellular wireless devices. We illustrate these methods with numerous examples, highlighting the tradeoffs in various chamber configurations. We conclude by calculating total radiated power and total isotropic sensitivity for a cellular-enabled wireless router and discuss methods for assessing uncertainty in estimates of these quantities.**

***Index Terms*—Cellular telecommunications, microwave measurement, reverberation chamber, wireless system.**

I. Introduction

While the smartphone immediately comes to mind when cellular technology is mentioned, modern cellular devices may take on a wide range of form factors to support machine-to-machine (M2M) and Internet of Things (IoT) applications. According to [1], there will be 11.5 billion mobile-connected devices by 2019, exceeding the world's projected population at that time (7.6 billion). The number of M2M devices is expected to grow faster than smartphones, from 495 million in 2014 to more than 3 billion by 2019. These devices may take on many different shapes and sizes, including parking kiosks, vending machines, routers, car dashboards, and the fast-growing area of wearables. The use of reverberation chambers for over-the-air testing of wireless devices with many form factors is on the rise for a number of reasons, including the ability to place objects practically anywhere within the working volume and the generally lower cost associated with reverberation chambers, as compared to anechoic chambers.

Over-the-air (OTA) certification tests are designed to ensure that devices on a given network will perform optimally and not interfere with other devices. Because cellular devices typically operate in multiple frequency bands and often have several, integrated antennas, such radiated tests are necessary. Reverberation chamber test procedures have been developed for tests in which angle-of-arrival information is not required, including total radiated power (TRP), total isotropic sensitivity (*i.e.*, receiver sensitivity, TIS), and data throughput for devices with multiple antennas [2]–[10].

Wireless device tests in which the received signal is demodulated in order to find metrics such as bit error rate (BER) or data throughput require that the channel conditions presented by the reverberation chamber setup are similar to those for which the equalizers in the receiver of the device-under-test (DUT) were designed to operate. Loading the reverberation chamber with RF absorber is often used to "flatten" the channel response. A channel that is not sufficiently flat with frequency (a "frequency-selective" channel) can distort the signal to the point where it cannot be demodulated [9], [11], [12].

Knowledge of the modulation format and bandwidth of the transmitted signal is helpful in deciding on the amount of loading required. For example, the cellular Band IV, using the LTE protocol, utilizes 10 MHz channel bandwidths, while Band II, using the W-CDMA air interface, utilizes channel bandwidths of approximately 4 MHz. However, the orthogonal frequency division multiplexed scheme in the LTE protocol requires frequency flatness over only a narrow bandwidth, on the order of but still exceeding ([9] and references therein) the occupied bandwidth of each independently transmitted subcarrier. Thus, more loading would be required for tests involving Band II than for Band IV even though the Band II channel is narrower.

Such intentional loading of reverberation chambers is somewhat counterintuitive to best practices developed by the EMC community [13], [14], where the goal is often to provide a uniform field (on average) at any location in the chamber. Such spatial uniformity results in a high quality factor Q, manifested by high maximum-to-minimum field values. However, loading is a necessity when receiver tests involving modulated signals are carried out.

Corona recognized the importance of loading early in his reverberation chamber work, particularly its importance to the isotropy of the chamber. In [15], he discusses the difference between distributed losses, such as wall surface absorption, versus concentrated loading, such as absorber pieces or apertures. He proposed using apertures with known areas and an assumed absorption coefficient of 1 as a way to determine the average wall loss absorption coefficient [15, eq. (2)]. This approach could be extended to additional discrete loss elements. Corona also recognized that wall loss typically is not the dominant loss mechanism for chambers built with highly conductive

Manuscript received February 1, 2016; revised March 9, 2016; accepted March 15, 2016. Date of current version April 27, 2016.

The authors are with the National Institute of Standards and Technology, Boulder, CO 80305 USA (e-mail: kate.remley@nist.gov; j.n.h.dortmans@student.tue.nl; cfw56@cornell.edu; robert.horansky@nist.gov; t.b.meurs@student.tue.nl jwang@boulder.nist.gov; dylan@boulder.nist.gov; holloway@boulder.nist.gov; pfw@boulder.nist.gov).

Color versions of one or more of the figures in this paper are available online at http://ieeexplore.ieee.org.

Digital Object Identifier 10.1109/TEMC.2016.2549031

walls [15, eq. (3)]. He used a thermodynamics approach to address this problem noting the similarity between thermodynamic equilibrium in a cavity and power equilibrium in a reverberation chamber. In [16], Corona extended the thermodynamics approach to the statistics of chambers with unstirred field components. While the unstirred components in [16] were generated by direct coupling between antennas, he noted that the new theory would be amenable to loaded chambers. This type of broad and creative thinking was a signature of Corona. The careful characterization of reverberation chamber loading to meet wireless test device needs is very much built on Corona's work.

Loading has the effect of increasing the correlation between static mode-stirring samples, including samples generated by frequency, position, or mechanical-paddle stirring. In the present work, we define "static mode-stirring sample" as a measurement sample acquired during the execution of a mode-stirring sequence under various static (stepped) conditions. Correlated samples contribute less efficiently to the estimate of the averaged quantity of interest. That is, uncertainty in the estimate will be higher for a given number of samples if the samples are significantly correlated. Also, because the absorber decreases the level of the stirred energy relative to unstirred energy within the chamber, the average spatial uniformity of the power density within the chamber is often diminished. This means that the measured quantity, estimated by averaging samples over a mode-stirring sequence, may now be a strong function of position within the chamber. Platform or position stirring, where the DUT is moved to various locations within the working volume of the chamber as part of the mode-stirring sequence, is often used to reduce uncertainty in the measured quantity caused by reduced spatial uniformity [10], [17], [18]. The increased setup and measurement complexity is a necessary tradeoff for the wireless community.

Prior work has focused on providing overviews of the theory, specific procedures, and uncertainty analyses [2]–[10], [17]. The contribution here is to provide an illustrated, step-by-step guide to setting up and verifying reverberation chambers for OTA testing of large and small cellular wireless devices based on current best practices. The methods described here are based on the verified assumption that the component of uncertainty that is related to the chamber setup is often dominated by the lack of spatial uniformity of the averaged fields in the chamber, as opposed to the number of samples in the mode-stirring sequence [10]. The number of mode-stirred samples tends to be high for wireless OTA tests in order to reduce uncertainties to acceptable levels such as those required by certification test plans [7], [8].

Our examples intentionally utilize a reverberation chamber having a single paddle and no platform, polarization, or antenna stirring (a configuration that generally would be considered suboptimal by the wireless test community) to illustrate methods for overcoming nonidealities due to configuration. The examples shown here are specific to cellular device testing. However, many of the setup concepts can be applied to test of other types of wireless devices that transmit digitally modulated communication signals.

This paper first provides a step-by-step guide to the many aspects of configuring a reverberation chamber for OTA testing.

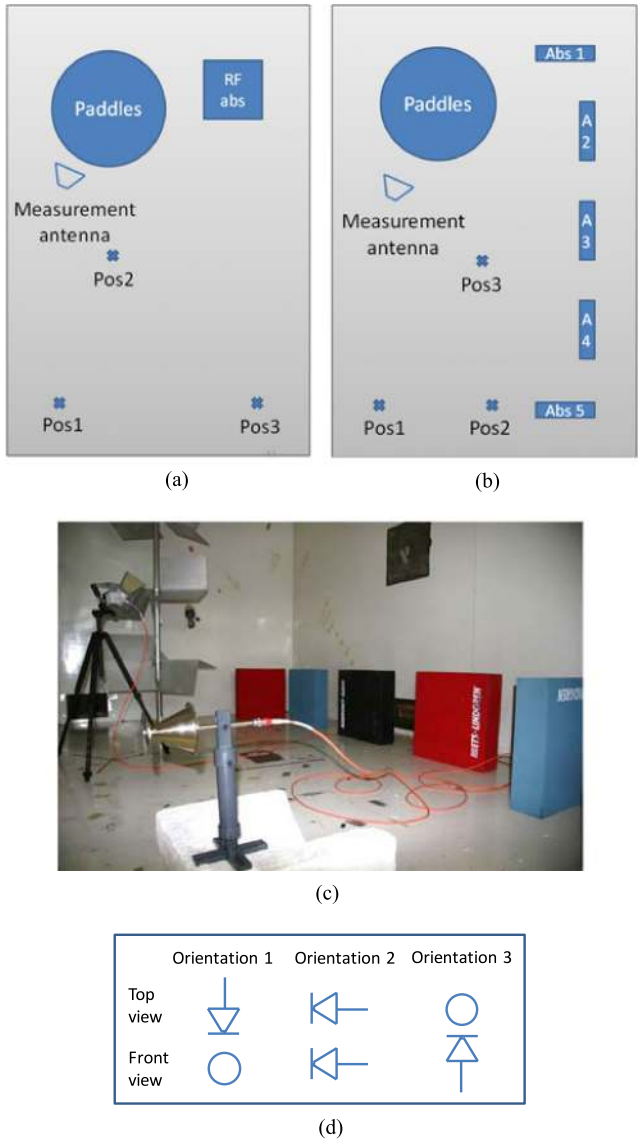

Fig. 1. Examples of configurations for OTA reverberation-chamber tests. Block diagrams in (a) and (b) show a top view of the chamber with (a) RF absorber stacked in the upper right corner and (b) placed on its side within the chamber. Omnidirectional transmit antenna positions "Pos 1"–"Pos 3" are denoted by the x symbols, and the directional receive (measurement) antenna is oriented toward the rotating paddles. (c) Photograph of configuration (b). At each transmit antenna position, three reference measurements were made with the three orthogonal orientations shown in (d).

We then provide methods for verifying that the environment provided by the reverberation chamber setup is as desired. Finally, we provide examples of actual device measurements, with a comparison to anechoic chamber measurements.

II. Preparing a Chamber Setup for OTA Testing

The chamber configuration, including the amount of RF absorber, the type and location of antennas within the chamber, their placement with respect to RF absorber, as well as the number and type of mode-stirring samples collected, will all have an effect on the uncertainty in the estimate of a quantity of interest. Example configurations are shown in Fig. 1.

TABLE I
MEASUREMENT CONFIGURATION FOR EXAMPLES PRESENTED IN THIS PAPER

Quantity	Value
Chamber specifications	
Interior dimensions	3.60 m × 4.27 m × 2.90 m
Paddle dimensions (cylindrical height × radius to tip of paddle)	Vertical paddle: 2.55 m × 38.5 cm
Transmit antenna (reference antenna)	Type: Biconical (omnidirectional) Frequency range: 0.65–3.5 GHz Height: 64 cm or 1.55 m* Location $P = 9$ positions in chamber
Receive antenna (measurement antenna)	Type: dual-ridge guide horn frequency range: 1–18 GHz Height: 1.0 m Location: Oriented toward paddle
Chamber configuration	
RF absorber (loading)	Each piece: 60 cm × 60 cm × 15 cm
Paddle positions	72 (5° steps)
Absorber configuration	Stacked or arranged on floor. See Fig. 1 for locations.
VNA measurement parameters	
Δf	50 kHz or 1 MHz, as noted in the text
All data: *BW*; f_c	1.4 GHz; 1.5 GHz
Cellular band: *BW*; f_c	100 MHz; 850 MHz
PCS band: *BW*; f_c	150 MHz; 1.925 GHz
IF bandwidth	1 kHz or 10 kHz, as noted in text
Frequency averaging	20 MHz (for visualization, noted in text when used)
Reference planes	Coaxial *N*-type connector at antenna input ports

* In Fig. 1, positions 2 and 3 were elevated (155 cm as opposed to 64 cm).

Because so many physical parameters are involved, configuring a chamber setup often requires an iterative approach, where chamber characteristics are assessed and the setup is modified as needed to provide desired channel characteristics for OTA testing.

In the following sections, we illustrate techniques for assessing the effects of the various setup parameters on the chamber measurements. For illustrative purposes, throughout this work we utilize the chamber setup and measurement parameters described in Table I, with the vector network analyzer (VNA) settings used for the reference measurements described in the following section.

A. Use of the Reference Power Transfer Function for Assessing the Chamber Setup

One common method for assessing the components of the chamber setup is by studying their effects on the "power transfer function" $G_{\rm ref}$. This quantity corresponds to the loss in the chamber for a given setup and is, ultimately, calibrated out during the measurement of a DUT (see Section IV-A). However, $G_{\rm ref}$ is a useful parameter for configuring the chamber setup because the DUT will experience approximately the same channel conditions as those obtained for the reference measurement. $G_{\rm ref}$ is often calculated from *S* parameter measurements as given in [10] and [17]:

$$G_{\rm ref} = \frac{1}{P}\sum_{p=1}^{P} \frac{\langle\langle |S_{21}(f,n,p)|^2\rangle_F\rangle_N}{\eta_M \eta_R \left(1-|\Gamma_M|^2\right)\left(1-|\Gamma_R|^2\right)}, \quad (1)$$

where the ensemble average (denoted by the chevrons) of the transmission parameter S_{21} is taken over *F* frequencies and *N* static mode-stirring samples, Γ_R and Γ_M are the free-space reflection coefficients of the reference and measurement antennas, respectively, and the radiation efficiency of each antenna (accounting for ohmic and dielectric losses) is given by η_R and η_M, respectively. These antenna efficiencies can be determined from separate measurements made in the reverberation chamber, see [19], *e.g.*, for details. To account for the reduced spatial uniformity of the average fields due to loading, $G_{\rm ref}$ is estimated from the average of $G_{{\rm ref},p}$ individual reference measurements made for *P* antenna positions.

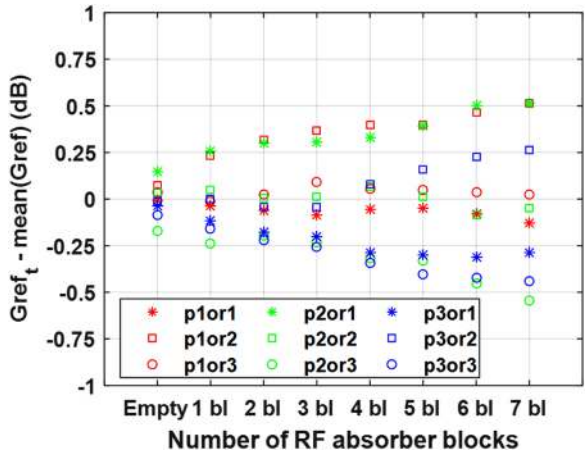

Fig. 2. Individual $G_{{\rm ref},p}$ measurements made for the chamber configuration in Fig. 1(a) with stacked absorber. Measured VNA data were averaged over the PCS band 1.85 GHz–2.0 GHz $\Delta f = 1$ MHz.

Fig. 2 shows typical variations in $G_{{\rm ref},p}$ measured at nine spatially uncorrelated antenna positions [20], [21] for the stacked-absorber configuration shown in Fig. 1(a). Measurements were conducted with various amounts of RF absorber loading the chamber. The range of $G_{{\rm ref},p}$ values obtained for each loading condition clearly illustrates the need for estimating $G_{\rm ref}$ from measurements made at multiple positions.

The variation in $G_{{\rm ref},p}$ values for a given setup can be described by the standard deviation of those measurements as

$$\sigma_{G_{\rm ref}} = \sqrt{\frac{1}{(P-1)}\sum_{p=1}^{P}\left(G_{{\rm ref},p} - G_{\rm ref}\right)^2}, \quad (2)$$

where, as above, *P* corresponds to a set of spatially uncorrelated reference-antenna locations at which $G_{{\rm ref},p}$ is determined from *S* parameter measurements made over a complete stirring sequence. $\sigma_{G_{\rm ref}}$ can be used to estimate the uncertainty due to lack of spatial uniformity of the averaged fields in the loaded chamber, as discussed in Section III-C and [10], [17], [22]. Replacing paddle positions with platform-stirring positions in the stirring sequence would typically result in a lower spread in the $G_{{\rm ref},p}$ values. We have intentionally used only mechanical paddle stirring in our examples to illustrate various concepts.

B. Configuring the Reverberation Chamber

As mentioned earlier, the placement and orientation of antennas, absorber, and DUTs in the reverberation chamber will have a significant effect on the uncertainty in the measured estimate

TABLE II
PARAMETERS FOR CHAMBER CONFIGURATIONS HAVING COMPARABLE CBWS BUT DIFFERENT ABSORBER ARRANGEMENTS IN THE PCS BAND (1.85–2.0 GHz)

	Distributed on floor: standing	Stacked	Distributed on floor: lying
CBW (MHz)	3.13	3.32	3.48
No. abs	3	7	4
G_{ref} (dB)	−29.46	−29.69	−29.78
$\sigma_{G_{\mathrm{ref}}}$ (dB)	0.15	0.30	0.35
K factor (dB)	−5.06	−4.36	−5.26

of the quantity of interest, as will the number of mode-stirring samples and type of mode-stirring mechanisms. The impact of the frequency response of the resulting configuration on the measured modulated signal must also be considered. Each of these parameters is discussed in the following sections.

1) Placement of Antennas Near Metallic Surfaces: In [23], Hill showed that, for an ideal unloaded chamber, the measured, averaged electromagnetic fields will be approximately uniformly distributed when the distance between the antenna and the metallic walls is greater than $\lambda/2$, where λ is the free-space wavelength in meters. Thus, the first step in configuring the placement of antennas, fixtures, DUTs, and absorber is that they are located more than $\lambda/2$ from the walls, floor, ceiling and other metal objects in the chamber.

2) Placement of RF Absorber: As discussed earlier, for OTA testing, it is usual to intentionally load the chamber to provide a frequency-flat channel for demodulation. The impact of loading in the chamber is a function of the exposed surface area of RF absorbing material in the chamber [18], [24], [25]. The more exposed surface area of RF absorber, the lower the spatial uniformity of the averaged fields in the chamber and the more position stirring that is typically used to compensate for that reduced uniformity. Because loading can increase the uncertainty in the estimate of the quantity of interest, the goal is often to find the minimum amount of absorber that can be utilized to obtain desired channel characteristics defined by the metrics in the following section.

RF absorber may be stacked in a single location or distributed throughout the chamber. Stacking RF absorber has the advantage of using less physical space in the chamber, but because less surface area is exposed for each block, more absorber may be required than when distributed throughout the chamber.

This effect is examined in Table II for three different absorber configurations. Chamber loading conditions that produced approximately the same coherence bandwidth (CBW) (defined in Section III-A) and the same G_{ref} value were determined for stacked absorber [see Fig. 1(a)], distributed absorber standing on its side [see Fig. 1(b)] and distributed absorber lying on its primary face. To maintain approximately the same CBW and G_{ref}, it was necessary to use different numbers of absorber blocks for each configuration because different surface areas were exposed. CBWs studied for each configuration were calculated from *S* parameter measurements made in the personal communication service (PCS) band (1.85–2.0 GHz).

Table II shows that $\sigma_{G_{\mathrm{ref}}}$, computed from (2) for $P = 9$ different antenna locations, is the largest for the absorber lying on the floor. Placing RF absorber on the walls or floor of the chamber reduces the metallic surface area of the chamber, making less stirred energy available at the receiver and decreasing the spatial uniformity. The second-largest standard deviation was obtained when the absorber was stacked. Similar trends were observed for other CBW values and for the cellular band frequencies (800–900 MHz). These results show that optimal use of distributed absorber, with the absorber placed away from the metal surfaces, can lead to lower uncertainty in the estimate of the quantity of interest for the same frequency flatness.

Note that, for this chamber setup, the *K* factor, which is defined as the ratio between the unstirred and stirred received power, cf. Section II-B4, does not follow an explicit trend as does $\sigma_{G_{\mathrm{ref}}}$. The *K* factor depends not only on loading but also on the type of antennas used, as discussed in Section II-B4. Note also that the exact placement of the RF absorber within the chamber will affect the value of $\sigma_{G_{\mathrm{ref}}}$. Consequently, the position of the RF absorber should be maintained for both the chamber characterization and DUT measurement steps.

3) Placement of Antennas Near Absorbing Surfaces (Proximity Effect): For a loaded chamber, it is also necessary to ensure that antennas are not placed too close to absorbing material. When an antenna is placed near to or oriented toward an RF-absorbing object, energy may be absorbed before undergoing mode stirring, which reduces the power coupled into the receive antenna. This systematic error, termed the "proximity effect" in [22] and [25], can, for example, result in a systematic underestimation of G_{ref}.

An empirical method for determining the significance of the proximity effect for a given setup was given in [22]. This method is based on multiple measurements of G_{ref} as the transmit (or receive) antenna is placed at increasingly far distances from the largest surface area of absorbing material in the chamber. Measurements are made over a complete stirring sequence and at multiple antenna locations *P* to account for the lack of spatial uniformity. If the difference between measurements at two increasingly large distances is below a specified threshold, the location of the antenna is deemed to be satisfactorily far from the absorbing material.

Fig. 3 illustrates an example set of proximity-effect measurements for the measurement parameters described in Table I with stacked absorber. The omnidirectional transmit antenna was moved increasingly far away from the stack of seven RF absorbing blocks. *S* parameter measurements were conducted over the stirring sequence at each of $P = 6$ antenna positions/orientation and G_{ref} was calculated. Table III shows the results of these measurements for the cellular band and the PCS band. Table III shows that for a difference threshold of 0.1 dB, for example, this antenna would need to be more than 1 m from the absorber.

4) Orientation of Antennas and Rician K Factor: The optimal orientation of the antennas in the chamber can be determined through the Rician *K* factor. In wireless-channel characterization, the *K* factor is a metric used to assess the ratio of signal components received via direct coupling between transmit and receive antennas to those received via reflections from objects in the environment (scattering) [11]. In a similar manner, for the reverberation chamber, we may define the *K* factor as the ratio

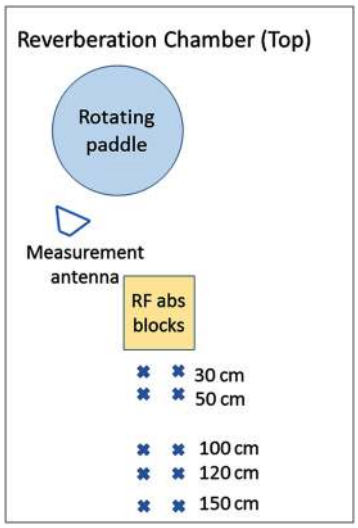

Fig. 3. Setup for proximity effect test. The transmit antenna was moved successively farther from the stack of RF absorber. Measurements at each distance were conducted at two locations with three antenna orientations at each location.

TABLE III
ILLUSTRATION OF PROXIMITY EFFECT FOR CHAMBER WITH SEVEN STACKED ABSORBERS, MEASURED IN THE CELLULAR (800–900 MHz) AND PCS (1.85–2.0 GHz) FREQUENCY BANDS

Distance to RF absorber (cm)	$G_{\rm ref}$ Cellular band (dB)	$G_{\rm ref}$ PCS band (dB)
30	−23.72	−31.20
50	−23.45	−30.79
100	−23.14	−30.66
120	−23.16	−30.60
150	−23.17	−30.42

of the unstirred received power P_u to the stirred received power P_s [26], [27] as

$$K = \frac{P_u}{P_s}. \tag{3}$$

This ratio may be approximated from the measured transmission coefficient as [26]

$$K \approx \frac{(|\langle S_{21}\rangle|)^2}{\langle |S_{21} - \langle S_{21}\rangle|^2\rangle}, \tag{4}$$

where $|\langle S_{21}\rangle|$ is the mean of S_{21} and $\langle |S_{21} - \langle S_{21}\rangle|^2\rangle$ is the variance of the real and imaginary components of S_{21} over all mode-stirring samples. Note that this equation was derived for an ideal unloaded chamber, but it is often used in the loaded case as well.

Higher values of *K* factor are generally undesirable because they are associated with a decrease in the spatial uniformity of the average fields within the chamber. Methods to analytically quantify this effect were studied in [10], [17], and [28].

For reverberation-chamber measurements, the *K* factor can take a range of values depending on several factors including the amount and placement of absorber, the radiation pattern of the antennas used in the measurement, and the antennas' location and orientation with respect to each other and the absorber.

Fig. 4 shows the *K* factor calculated from (4) for various absorber amounts in the stacked loading condition [see Fig. 1(a)].

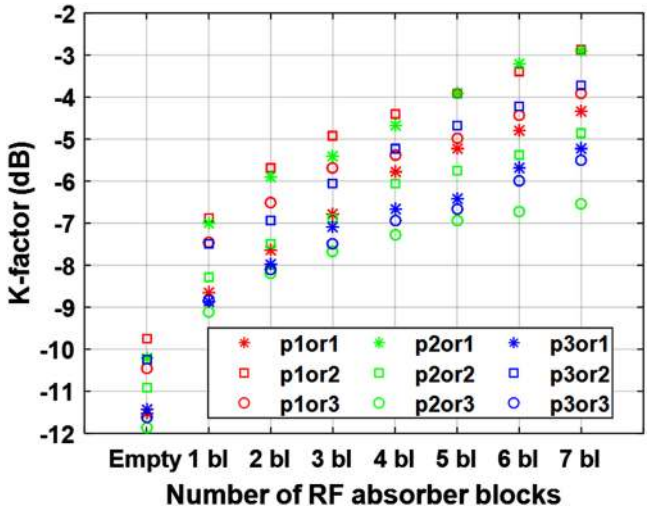

Fig. 4. Rician *K* factor calculated from (4) for measurements made at three omnidirectional transmit antenna locations and three orientations for each location (see Fig. 1 (a)). The antenna setup was described in Table I with $\Delta f = 1$ MHz. Results were averaged over the PCS band, 1.85–2.0 GHz.

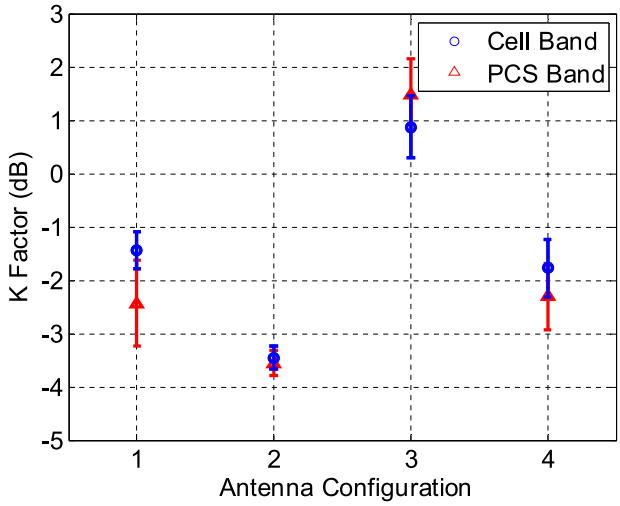

Fig. 5. *K* factor for four different antenna configurations in a heavily loaded chamber. Antenna TX/RX pairs consisted of: 1. directional/directional; 2. omnidirectional/directional; 3. directional/omnidirectional; 4. omnidirectional/omnidirectional. Measurements were made in the cellular band (circles) and the PCS band (triangles) with $\Delta f = 1$ MHz.

We see that the spread in *K* factor values increases between the unloaded and loaded conditions. For this setup, the lowest *K* factor was achieved when the reference antenna was behind the measurement antenna (position 1, orientation 2). The highest *K* factor was obtained when the reference antenna was near to the measurement antenna (at position 2, orientation 3). Such information can be useful in determining the optimal placement of antennas for a given chamber setup.

Fig. 5 illustrates the effect of the antenna radiation pattern on the *K* factor. Measurements were made in a heavily loaded reverberation chamber (stack of 14 RF absorbers) with all other measurement parameters given in Table I. Six $G_{\rm ref}$ measurements were made, where each value of $G_{\rm ref}$ consisted of $P = 9$ different reference antenna heights and polarizations.

Fig. 5 shows that, for this configuration, both the *K* factor and its variance were lowest when an omnidirectional transmit

antenna was used to excite the chamber and a directional receive antenna was aimed toward the rotating paddle near the corner of the chamber. This configuration results in low direct coupling between the TX and RX antennas, as would directional TX and RX antennas aimed away from each other. However, unlike a directional TX antenna aimed at the wall, the omnidirectional TX antenna causes a greater amount of stirred energy to be incident on the directional RX antenna, resulting in a lower *K* factor. In [22], we showed that this lowest-*K*-factor configuration also resulted in the lowest value of $\sigma_{G_{\rm ref}}$. Note that most cellular devices utilize omnidirectional azimuthal radiation patterns, which further motivates the use of an omnidirectional reference transmit antenna. Other techniques for reducing the *K* factor include use of cross polarized antennas or physically blocking the line of sight between two antennas [17].

C. Choice of Mode-Stirring Sequence

The number and type of mode-stirring samples that comprise the stirring sequence may be considered as part of the reverberation-chamber setup. The sequence is often chosen based upon logistical factors as well as desired accuracy. For example, while use of a very large number of stirring samples would improve the estimate of the quantity of interest, this would not be efficient in terms of measurement time.

As mentioned in Section II-A, for loaded chambers, position stirring is often used to average out the effects of the lack of spatial uniformity. Even though the variation in the measured samples may be significant from position to position, the averaged results still typically converge to a single, "correct" value if the setup has been verified and if the quantity of interest is not highly nonlinear. Both conditions are usually met for cellular device testing.

To efficiently obtain an estimate of the quantity of interest, uncorrelated mode-stirring samples are typically chosen. Numerous references discuss methods for determining the effective number of independent samples *e.g.*, [29]–[33]. Other work discusses methods for determining uncertainty in reverberation-chamber measurements when correlation between samples exists and when the *K* factor is nonnegligible [10], [17], [28].

Fig. 6 shows an example of a measurement in which an increasing number of paddle positions is used. The relative uncertainty, given by $\sigma_{G_{\rm ref}}/\sqrt{MN}$, where *M* refers to the number of platform positions and *N* to the number of paddle angles, deviates from that expected for uncorrelated samples for a large sample number. The uncertainty in the ideal "ergodic-mode" case [29] decreases by $1\Big/\sqrt{MN}$ (simply *N* in our example setup of Table I because only paddle stirring is used). See [28] for more information on the use of correlated samples in uncertainty calculations.

D. Frequency Averaging and the Chamber's Frequency Response

Because cellular wireless devices transmit modulated signals, quantities of interest such as radiated power or receiver sensitivity are estimated from measurements that are averaged over the signal bandwidth. Such averaging or "frequency stirring" often results in decreased uncertainty in the estimate of the quantity of interest as compared to reverberation-chamber measurements of single-frequency quantities such as electric field. However, because the chamber response can vary significantly over the modulation bandwidth of the signal, it is important to understand whether this response will impact the values derived from measurement.

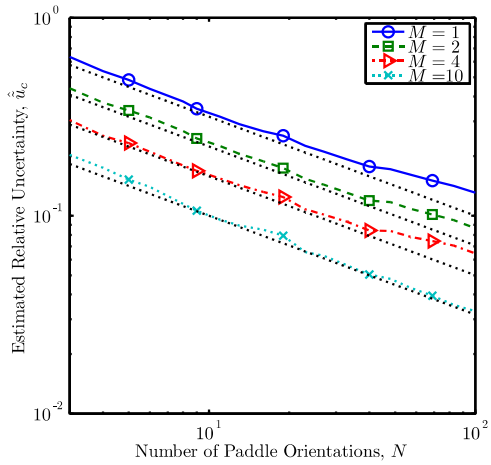

Fig. 6. Relative uncertainty (defined in the text) for reverberation-chamber measurements of the transfer function for an increasing number of *N* paddle angles for various values of *M* antenna locations. The symbols represent every 20th data point. The dotted lines without symbols represent the dependence $1/\sqrt{MN}$ given in [29] (from [28]).

This is illustrated in Fig. 7(a), where we have plotted individual mode-stirring samples of $|S_{21}|^2$ (thin lines), and those averaged over 72 paddle angles and nine antenna locations (thick lines) for an unloaded chamber and a chamber loaded with seven stacked absorber blocks. The frequency step was 50 kHz. See Table I for other measurement parameters. We see a less rapid variation in $|S_{21}|^2$ as a function of frequency for the loaded chamber due to frequency correlation. Due to this correlation, measurements made over a limited bandwidth, a 4 MHz channel, for example, may be subject to a higher value of $\sigma_{{\rm Gref},p}$. Quantifying this effect helps to determine whether the number of mode-stirring samples is adequate for a given setup.

The thicker dash-dotted lines in Fig. 7(a) and (b) show a linear regression carried out over the PCS frequency band for each loading condition. The frequency roll-off is approximately 0.5 dB for both the unloaded and loaded chambers. Also shown in Fig. 7(b) is the frequency response for low-, mid-, and high-band channels, denoted by the short horizontal black lines. These were calculated as the average of the linear regression curve over the 4 MHz channel. As illustrated in Fig. 7(b), if the chamber's reference power transfer function was calculated as the mean of the regression curve calculated over the whole PCS band, while the DUT was measured for a channel near the lower edge of the PCS band, the reference loss could be overestimated. This motivates the determination of a different $G_{\rm ref}$ value for each channel, as discussed in Section IV.

III. Verifying the Chamber Setup

As discussed earlier, for measurements in which the signal must be demodulated, such as for receiver sensitivity

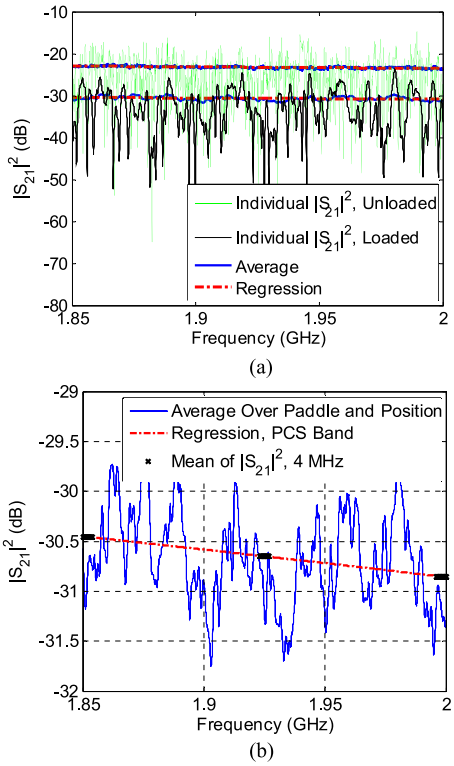

Fig. 7. In (a), a single mode-stirring sample of $|S_{21}|^2$ as a function of frequency for the unloaded chamber (light green curve) and for the loaded chamber (thin black curve). The average over 72 paddle angles and nine antenna positions is shown by the thick blue curves, and a linear regression is shown by the red dashed lines. In (b), the averaged, regression of the loaded chamber response shows a decrease of ~0.5 dB over the PCS band. Individual 4 MHz channels are shown by the short, horizontal black lines, illustrating the necessity of frequency averaging.

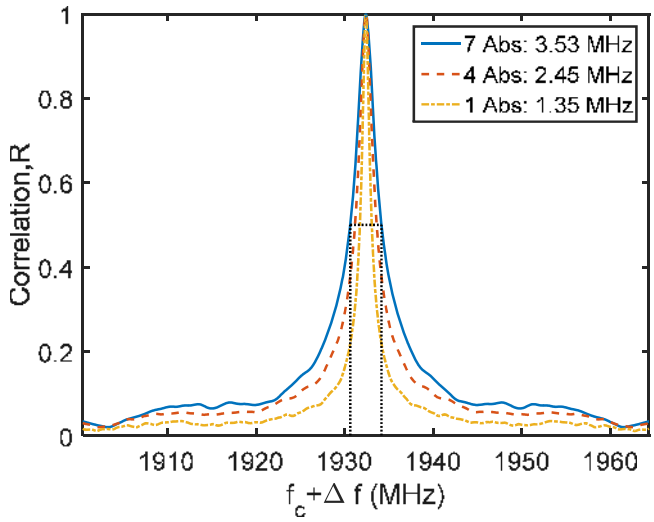

Fig. 8. Average frequency correlation *R* of the channel corresponding to the reverberation chamber setup for three loading conditions. *R* was found from *S* parameter measurements made over a 150 MHz bandwidth centered at the middle of the PCS band. The CBW corresponding to a threshold of 0.5 for the various loading conditions is shown in the legend.

measurements, it is important that the chamber is configured to minimize the possibility that the device erroneously reports quantities of interest. Metrics used to assess the channel created by the reverberation chamber include the coherence bandwidth (CBW, related to the frequency band over which the channel is "frequency flat"), the root-mean-square (RMS) delay spread (τ_{RMS}, related to the ring-down time of the chamber), and the spatial uniformity of the proposed setup (related to the measurement uncertainty). Because CBW and τ_{RMS} are inversely related, many test procedures specify only one or the other, and then require determination of the spatial uniformity.

In the following discussions of these three metrics (CBW, τ_{rms}, and $\sigma_{G_{\mathrm{ref}}}$), the *S* parameter measurements used to illustrate these metrics were again made with a configuration similar to that illustrated in Fig. 1(a) and having the characteristics given in Table I. Estimating these metrics from measured data depends on parameters such as the number of frequency points and the bandwidth used for the measurements. This is discussed next.

A. Coherence Bandwidth

The CBW metric describes the average bandwidth over which the frequency components have a minimum specified level of correlation [12], [34], [35]. Correlation between frequency components reduces the frequency selectivity of the channel, which, as discussed earlier, is often desirable for demodulation of the signal. Such correlation was illustrated in Fig. 7(b) by the slower variation as a function of frequency than that observed for the unloaded chamber in Fig. 7(a).

The CBW is often determined by assessing the level of correlation between frequencies over a specified bandwidth, *BW* (for example, the PCS band). One common method is to calculate the autocorrelation function, r, of the frequency-domain transfer function S_{21} for several frequency offsets (lags) Δf_i ranging from $f_c - BW$ to $f_c + BW$, where f_c is the center frequency. If uncorrelated, such autocorrelations should be near zero for all values of Δf_i. If correlated, then one or more of the autocorrelations will be significantly nonzero. For reverberation-chamber measurements, the autocorrelation $r(\Delta f_i, n)$, calculated for the *i*th frequency offset Δf_i and mode-stirring sample n, may be given as [35, Section 1.3.5.12]

$$r\left(\Delta f_i, n\right) = \sum_{j=1}^{M} S_{21}\left(f_j, n\right) S_{21}^{*}\left(f_j + \Delta f_i, n\right) \qquad (5)$$

where $S_{21}\left(f, n\right)$, and the complex conjugate S_{21}^{*} are vectors of the complex transmission parameter measured at M frequency points, f_j, within the bandwidth of interest, BW, so that $f_1 = f_c - BW/2$ and $f_M = f_c + BW/2$. The resulting $I \times N$ matrix is averaged over all paddle positions, n, to obtain a vector *R* of length *I* corresponding to the average autocorrelation coefficient calculated at each frequency offset.

An example showing the average autocorrelation, *R*, is plotted in Fig. 8. The frequency step of the VNA was 50 kHz. The result was found by averaging the vector of correlation coefficients *r* over all $N = 72$ paddle angles.

The bandwidth over which the frequency components are deemed to be "correlated" may be found as the band above a specified threshold. The higher the threshold, the flatter the channel over a given bandwidth. See [12] and [35] for more

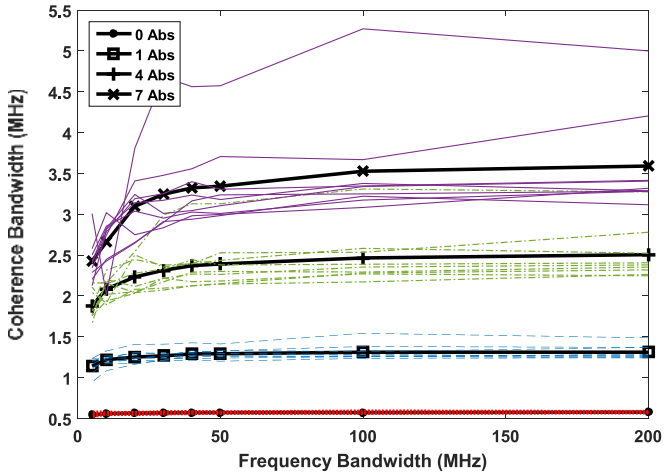

Fig. 9. CBW calculated over different frequency bandwidths for 0-, 1-, 4-, and 7-absorber loading conditions (indicated by the symbols). For each loading condition, individual measurements made at nine antenna locations are shown by the thin lines, and the mean is shown by the thicker line.

information on this. The choice of the correlation threshold will typically depend on the type of receiver used. For example, lower threshold values may be specified for testing conducted on commercially available cellular devices because error correction is used. Threshold values vary, with 1/*e*, 0.707, and 0.5 as common values. In the present work, we use a threshold of 0.5.

Because CBW is a derived metric, both the number of points and the bandwidth over which it is estimated will affect the result. Fig. 9 shows the effect of the frequency bandwidth over which the CBW is calculated on the estimate of the CBW. VNA measurements were conducted with the setup described in Table I at nine antenna positions (three locations and three orientations at each location) for four loading cases. The frequency step was 50 kHz. The unloaded chamber is represented by the lower curves and the 1-, 4-, and 7-absorber cases are represented by the successively higher curves. We see that the CBW increases with loading, as expected, and that the variance in the estimate of the CBW increases with loading, as shown by the increased spread in the lines corresponding to each antenna location. This increase in variance is due to the reduced uniformity of the averaged fields caused by loading.

Fig. 9 shows that if the CBW is not calculated over a sufficiently wide frequency bandwidth, the VNA measurement will underestimate the CBW. Likewise, an insufficient number of frequency points used to calculate CBW can result in erroneous values of CBW.

B. RMS Delay Spread

The RMS delay spread is a metric describing how quickly reflections decay in a given multipath propagation environment [11], [36]. Similar to the CBW, it may be used to verify the reverberation configuration, with shorter RMS delay spread values corresponding to increased loading. This metric is calculated in the time domain.

For the *n*th stepped mode-stirring sample measured at τ_n, the impulse response of the chamber setup may be estimated from the inverse Fourier transform of the measured *S* parameters $h_n\,(t) \cong \mathrm{IFFT}\,\{S_{21}\,(f,n)\}$. The magnitude squared of the impulse response corresponds to the power delay profile (PDP)

$$PDP\,(t) = \langle |h(t,\tau_n)|^2 \rangle \tag{6}$$

where $h\,(t,\tau_n)$ is the *n*th mode-stirring sample of the linear, time-varying impulse response of the channel and the chevrons denote the ensemble average. The RMS delay spread is found from the square root of the second central moment of the *PDP* as

$$\tau_{\mathrm{rms}} = \sqrt{\frac{\int_0^\infty (t-t_0)^2\, PDP\,(t)\,dt}{\int_0^\infty PDP\,(t)\,dt}} \tag{7}$$

where t_0 is the mean delay of the propagation channel given by

$$t_0 = \frac{\int_0^\infty t PDP\,(t)\,dt}{\int_0^\infty PDP\,(t)\,dt} \tag{8}$$

see [11] and [36] for a more detailed explanation, with [36] focusing on making these measurements in reverberation chambers.

The RMS delay spread corresponding to a reverberation chamber setup can be tuned to match specific real-world propagation environments by changing the loading. For example, the "NIST model," derived from measurements made in several building-penetration scenarios [37] specifies an 80 ns RMS delay spread and has been proposed for use in some cellular standards [7]. Values of RMS delay spread from NIST building penetration measurements in various locations ranged from less than 20 ns for an apartment building to around 400 ns in a high rise office building at 900 MHz [38].

As with CBW, the number of points and the frequency bandwidth over which the calculation is made will affect the accuracy of the estimate of τ_{rms}. These values will depend on the carrier frequency, loading, and antenna setup. Values of τ_{rms} calculated for the same loading conditions in Fig. 9 are shown in Fig. 10, where we again see that calculation over a narrow bandwidth may lead to erroneous values.

C. Spatial Uniformity

As discussed in Section II-A, the standard deviation of reference measurements made at several locations throughout the chamber is given by $\sigma_{G_{\mathrm{ref}}}$. This quantity may be used to assess the uncertainty due to lack of spatial uniformity in the estimate of both G_{ref} and the DUT quantities of interest [10], [22]. Note that each chamber loading configuration may result in a different power transfer function and a different $\sigma_{G_{\mathrm{ref}}}$ (see Table II). As a result, verifying this aspect of the chamber setup is typically carried out for each loading configuration.

As with CBW and τ_{rms}, the determination of $\sigma_{G_{\mathrm{ref}}}$ for a given setup depends on the bandwidth over which the calculation is performed and the number of frequency points within that bandwidth. For measurements of modulated signals used in cellular applications, the bandwidth is fixed by the channel to be tested. Thus, the user must ensure that an adequate number of frequency

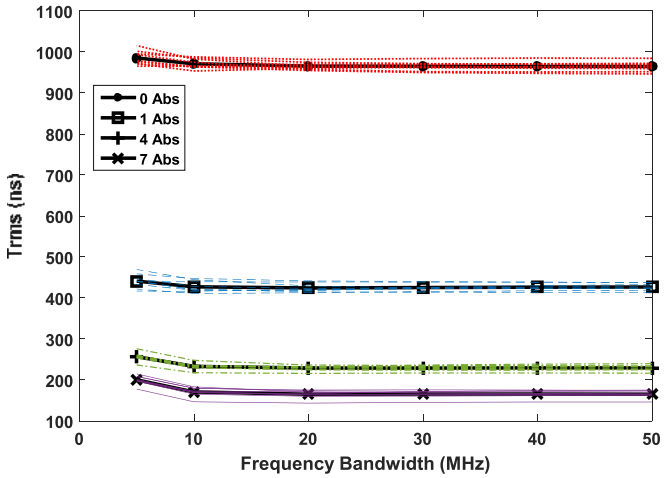

Fig. 10. τ_{rms} calculated over different frequency bandwidths for 0-, 1-, 4-, and 7-absorber loading conditions (indicated by the symbols). For each loading condition, individual measurements made at nine antenna locations are shown by the thin lines, and the mean is shown by the thicker line.

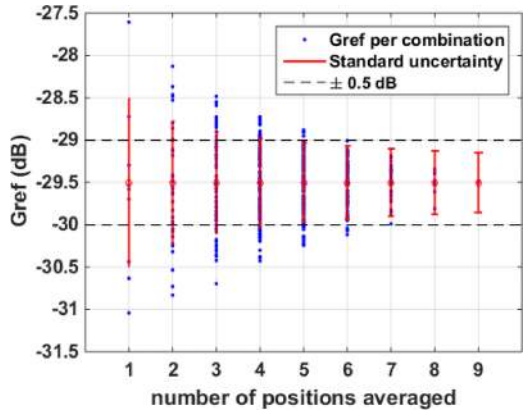

Fig. 11. Reference power transfer function calculated from (1) for PCS channel 9262 (1.850–1.854 GHz). VNA measurements were made at nine spatially uncorrelated antenna positions with $\Delta f = 1\,\mathrm{MHz}$. Values of G_{ref} and $u_{G_{\mathrm{ref}}}$ were then calculated for various combinations of these nine sets of data.

samples are measured for estimating G_{ref} and $\sigma_{G_{\mathrm{ref}}}$. Once $\sigma_{G_{\mathrm{ref}}}$ has been determined, the component of uncertainty due to lack of spatial uniformity may then be calculated as [10], [22]

$$u_{G_{\mathrm{ref}}} = \frac{\sigma_{G_{\mathrm{ref}}}}{\sqrt{P}}. \tag{9}$$

Note that $u_{G_{\mathrm{ref}}}$ is estimated solely from the variance in G_{ref}, which is found over P antenna positions, as opposed to the number of mode-stirring samples. Based on a significance test [10], it was determined that the variation due to lack of spatial uniformity was the dominant component of uncertainty in an estimate of G_{ref} for all loading cases except when a very small number of mode-stirred samples were used.

To understand why the value of $P = 9$ is generally used to calculate this component of uncertainty, Fig. 11 shows G_{ref} calculated from (1) for various subsets of $P = 9$ spatially uncorrelated antenna positions and orientations. All permutations of the nine measurements were combined to estimate G_{ref}. The

TABLE IV
REFERENCE POWER TRANSFER FUNCTION G_{ref} AND STANDARD DEVIATION $\sigma_{G_{\mathrm{ref}}}$ FOR VARIOUS LOADING CONDITIONS

No. RF abs.	CBW (MHz)	G_{ref} PCS (dB)	$\sigma_{G_{\mathrm{ref}}}$ PCS (dB)	G_{ref} PCS 9262 (dB)	$\sigma_{G_{\mathrm{ref}}}$ PCS 9262 (dB)	G_{ref} PCS 9662 (dB)	$\sigma_{G_{\mathrm{ref}}}$ PCS 9662 (dB)
4	2.33	-28.23	0.30	−27.97	0.61	−28.05	0.55
6	3.01	−29.33	0.37	−29.03	0.67	−29.18	0.64
7	3.35	−29.81	0.41	−29.37	0.92	−29.72	0.67
8	3.68	−30.30	0.45	−29.83	0.91	−30.25	0.66

Col. 1: Number of RF absorber blocks.
Col. 2: CBW with a 0.5 threshold.
Cols. 3 and 4: Full PCS band (1850–2000 MHz).
Cols. 5 and 6: PCS Uplink Channel 9262 (1850–1854 MHz).
Cols. 7 and 8: PCS Downlink Channel 9662 (1930–1934 MHz).
$\Delta f =$ 1 MHz, 72 paddle positions and 9 reference antenna locations.

reverberation chamber setup was again that described in Table I with seven RF absorbers stacked [see Fig. 1(a)]. Measurements were made in PCS channel 9262 (1.850–1.854 GHz). Fig. 11 illustrates that $P = 9$ antenna positions are adequate for obtaining a $u_{G_{\mathrm{ref}}}$ value that is lower than 0.5 dB, as required in [8].

IV. DUT MEASUREMENTS

Once the chamber has been configured and the setup verified in terms of its channel characteristics (assessed by the CBW or τ_{rms}) and uncertainty due to lack of spatial uniformity, OTA tests may be conducted with confidence. We focus on two common tests used to certify the performance single-input, single-output cellular wireless devices: TRP and TIS [7], [8].

A. Reference Power Transfer Function

Both TRP and TIS require knowledge of the true power at the DUT, which requires that the loss within the chamber and antennas be calibrated out. To do this, prior to calculating the TRP or TIS value, the chamber's reference power transfer function is determined for the chamber setup verified in the previous sections. For example, to test a 3.84 MHz W-CDMA signal, the chamber is loaded to provide a CBW of approximately 3.84 MHz.

Finding the correct loading may be done empirically, by loading the chamber and computing the CBW or τ_{rms} for increasing amounts of absorber until the desired characteristics are achieved. Table IV provides representative values of CBW, G_{ref} and $\sigma_{G_{\mathrm{ref}}}$ for the NIST chamber configuration in Table I with stacked absorber [Fig. 1(a)] and $\Delta f = 1$ MHz. Note that the standard deviation increases significantly when calculations are made over the channel's bandwidth (as opposed to the entire cellular or PCS bands as shown in Table II).

The value of G_{ref} that corresponds to the loading that provides the desired CBW is then used in formulas for TRP and TIS to compensate for loss in the chamber setup.

Objects such as RF absorber, fixtures, and antennas are often left in the chamber for both the reference and DUT measurements. This is done so that the DUT experiences approximately the same channel as that for which the reference measurements were made. Note that the removal of metallic fixtures and

antennas from the chamber will typically have little effect on the uncertainty in the estimate of the quantity of interest.

B. Total Radiated Power

The total power radiated by the DUT may be estimated from measurement as [10], [17]

$$P_{\mathrm{TRP}} = \frac{1}{R}\sum_{r=1}^{R} \frac{\langle P_{\mathrm{Meas}}\rangle_N \left|1-\Gamma_{\mathrm{M}}\Gamma_{\mathrm{RX}}\right|^2}{\eta_{\mathrm{M}}(1-|\Gamma_{\mathrm{M}}|^2)G_{\mathrm{ref}}} \tag{10}$$

where $\langle P_{\mathrm{Meas}}\rangle_N$ is the ensemble average of power samples measured by a base station emulator (BSE) or spectrum analyzer over the same *N*-sample mode-stirring sequence that was used for the reference measurement (*e.g.*, the same paddle angles and platform positions). The term $\left|1-\Gamma_{\mathrm{M}}\Gamma_{\mathrm{RX}}\right|^2$ corrects for the impedance mismatch between the measurement antenna and the receiver assembly, where Γ_{RX} is the reflection coefficient of the receiver assembly, and Γ_{M} is the free-space reflection coefficient of the measurement antenna. As before, η_{M} is the radiation efficiency of the measurement antenna.

Note that if additional cables or adapters are used for the power measurement that were not used in the reference measurement, they will need to be de-embedded. Procedures for this were outlined in the Appendix of [10].

P_{TRP} is computed from the average of a set of $\langle P_{\mathrm{Meas}}\rangle_N$ measurements made for *R* DUT antenna positions (similar to the *P* antenna positions for the reference measurement). Note that the *R* DUT measurement positions do not need to be the same as the *P* reference measurement positions as long as the measurements are carried out within the volume for which the chamber setup was verified. Often, $R = 1$ for measurements made by test labs to save time.

As discussed in Section III-C, position averaging significantly improves the estimate of TRP. Thus, for most commercially available reverberation chambers used for OTA testing, multiple spatially dependent stirring mechanisms are used (such as platform and/or antenna polarization stirring).

C. Total Isotropic Sensitivity

The total isotropic sensitivity P_{TIS} is the power estimated to be at the input port of the DUT's antenna when it reports a specified maximum acceptable BER (for example, 1.2% for the W-CDMA standard). P_{TIS} may be given by

$$P_{\mathrm{TIS}} = \frac{\eta_{\mathrm{M}}\left(1-|\Gamma_{\mathrm{M}}|^2\right)}{R\left|1-\Gamma_{\mathrm{M}}\Gamma_{\mathrm{RX}}\right|^2}\sum_{r=1}^{R}\frac{G_{\mathrm{ref},r}}{N}\left(\sum_{n=1}^{N}\frac{1}{P_{\mathrm{BSE}}(n)}\right)^{-1} \tag{11}$$

where $P_{\mathrm{BSE}}(n)$ corresponds to the power emitted from the BSE when the DUT reports the threshold bit-error rate. As with TRP, the estimate of TIS may be improved by the use of position stirring, as found in many commercial implementations. In practice, $G_{\mathrm{ref},r}$ is often approximated from a single value of G_{ref} to save time. Note that, per [7], [8], the harmonic mean is used to calculate the average value of the BSE's output power, while the arithmetic mean is used for G_{ref}. The harmonic mean minimizes the effects of outliers. Other averaging arrangements may be used as well. Variability in TIS, as a function of position, is similar to that found for TRP for the chamber configuration used.

TABLE V
TRP AND TIS FOR A WIRELESS ROUTER MEASURED FOR W-CDMA SIGNALS IN THE CELLULAR AND PCS BANDS

Frequency band	DUT test	NIST RC (dBm)	AC 1 (dBm)	AC 2 (dBm)
Cellular	TRP	20.35	22.14	20.59
	TIS	−107.72	−109.08	−108.65
PCS	TRP	19.43	20.28	19.81
	TIS	−106.51	−108.98	−110.04

In Table V, we present a comparison between TRP and TIS measurements made for a wireless router. For the reverberation chamber results, the TIS was measured at $R = 9$ locations for the seven stacked absorber case shown in Fig. 1(a). We see that agreement between RC and AC measurements is within 2 dB for TRP measurements and within 4 dB for TIS measurements. A similar level of agreement is shown between the two anechoic chambers.

V. CONCLUSION

Loading has the effect of reducing the amplitude and phase variation of the channel presented to the DUT, which better replicates the channel in which many receivers were designed to operate. Under loaded conditions, the chamber setup must be carefully configured and verified before proceeding with the DUT measurements of TRP and TIS. Such step-by-step guidance was described here.

ACKNOWLEDGMENT

The authors are grateful to the members of the CTIA's Wireless Internet of Things W-IoT subgroup for interesting discussions of the "real-world" issues facing the wireless test and measurement community. Participating test labs for this work include Cisco Systems, Inc., and SGS North America, Inc.

REFERENCES

[1] Cisco Visual Networking Index. (2014, Feb.). *Global Mobile Data Traffic Forecast Update, 2014*, San Jose, CA, USA. [Online]. Available: http://www.cisco.com/c/en/us/solutions/collateral/serviceprovider/visual-networking-index-vni/white_paper_c11-520862.htm

[2] P.-S. Kildal and K. Rosengren, "Correlation and capacity of MIMO systems and mutual coupling, radiation efficiency and diversity gain of their antennas: Simulations and measurements in reverberation chamber," *IEEE Commun. Mag.*, vol. 42, no. 12, pp. 102–112, Dec. 2004.

[3] O. Delangre, P. De Doncker, F. Horlin, M. Lienard, and P. Degauque, "Reverberation chamber environment for testing communication systems: Applications to OFDM and SC-FDE," in *Proc. 68th IEEE Veh. Technol. Conf.*, Calgary, Canada, Sept. 2008, pp. 1–5.

[4] V. Monebhurrun and T. Letertre, "Total radiated power measurements of WiFi devices using a compact reverberation chamber," in *Proc. 20th Int. Zurich Symp. Electromagn. Compat.*, 2009, pp. 65–68.

[5] P.-S. Kildal, C. Orlenius, and J. Carlsson, "OTA testing in multipath of antennas and wireless devices with MIMO and OFDM," *Proc. IEEE*, vol. 100, no. 7, pp. 2145–2157, Jul. 2012.

[6] C. Lötbäck Patané, A. Skårbratt, R. Rehammar, and C. Orlenius, "On the use of reverberation chambers for assessment of MIMO OTA performance of wireless devices," in *Proc. 7th Eur. Conf. Antennas Propag.*, Gothenburg, Sweden, pp. 101–105, Apr. 2013.

[7] 3rd Generation Partnership Project, *Technical Specification Group Radio Access Networks; Universal Terrestrial Radio Access (UTRA) and Evolved*

Universal Terrestrial Radio Access (E-UTRA); Verification of Radiated Multi-antenna Reception Performance of User Equipment (UE), rel. 12, 3GPP TR 37.977 v1.3.0, Nov. 2013.

[8] CTIA Certification, *Test Plan for Wireless Device Over-the-Air Performance—Method of Measurement for Radiated RF Power and Receiver Performance, Large-Form-Factor Integrated Device Addendum (Accepted)*, Dec. 2014.

[9] D. Micheli, M. Barazzetta, F. Moglie, and V. M. Primiani, "Power boosting and compensation during OTA testing of a real 4G LTE base station in reverberation chamber," *IEEE Trans. Electromagn. Compat.*, vol. 57, no. 4, pp. 623–634, Aug. 2015.

[10] K. A. Remley, C.-M. Wang, R. J. Pirkl, A. T. Kirk, J. Aan Den Toorn, D. F. Williams, C. L. Holloway, J. A. Jargon, and P. D. Hale, "A significance test for reverberation-chamber measurement uncertainty in total radiated power of wireless devices," *IEEE Trans. Electromagn. Compat.*, vol. 58, no. 1, pp. 207–219, Oct. 2015.

[11] A. Goldsmith, *Wireless Communications*. Cambridge, England: Cambridge Univ. Press, 2005.

[12] K. A. Remley, S. J. Floris, H. A. Shah, and C. L. Holloway, "Static and dynamic propagation-channel impairments in reverberation chambers," *IEEE Trans. Electromagn. Compat.*, vol. 53, no. 3, pp. 589–599, Aug. 2011.

[13] *Joint Task Force IEC SC77B-CISPR/A, Electromagnetic Compatibility (EMC)—Part 4.21: Testing and Measurement Techniques—Reverberation Chamber Test Methods*, IEC 61000-4-21, Geneva, Switzerland, Aug. 2003.

[14] D. A. Hill, *Electromagnetic Fields in Cavities: Deterministic and Statistical Theories*, Piscataway, NJ, USA: Wiley-IEEE Press, 2009.

[15] P. Corona, G. Latmiral, and E. Paolini, "Performance and analysis of a reverberating chamber with variable geometry," *IEEE Trans. Electromagn. Compat.*, vol. 22, no. 1, pp. 2–5, Feb. 1980.

[16] P. Corona, G. Ferrara, and M. Migliaccio, "Reverberating chamber electromagnetic field in presence of an unstirred component," *IEEE Trans. Electromagn. Compat.*, vol. 42, no. 2, pp. 111–115, May 2000.

[17] P.-S Kildal, X. Chen, C. Orlenius, M. Franzen, and C. Lötbäck Patané, "Characterization of reverberation chambers for OTA measurements of wireless devices: Physical formulations of channel matrix and new uncertainty formula," *IEEE Trans. Antennas Propag.*, vol. 60, no. 8, pp. 3875–3891, Aug. 2012.

[18] S. van de Beek, K. A. Remley, C. L. Holloway, J. M. Ladbury, and F. Leferink, "Characterizing large-form-factor devices in a reverberation chamber," in *Proc. EMC Europe Int. Symp. Electromagn. Compat Dig.*, Sept. 2–6, 2013, pp. 375–380.

[19] C. L. Holloway, H. A. Shah, R. J. Pirkl, W. F. Young, D. A. Hill, and J. Ladbury, "Reverberation chamber techniques for determining the radiation and total efficiency of antennas," *IEEE Trans. Antennas Propag.*, vol. 60, no. 4, pp. 1758–1770, Apr. 2012.

[20] N. Janssen, K. A. Remley, C. L. Holloway, and W. F. Young, "Correlation coefficient and loading effects for MIMO antennas in a reverberation chamber," in *Proc. Int. Symp. Electromagn. Compat.*, 2013, pp. 514–519.

[21] W. C. Jakes, *Microwave Mobile Communications*, 2nd ed. New York, NY, USA: Wiley, 1994.

[22] J. Aan Den Toorn, K. A. Remley, C. L. Holloway, J. M. Ladbury, and C.-M. Wang, "Proximity-effect test for lossy wireless-device measurements in reverberation chambers," *IET Sci. Meas. Technol.*, vol. 9, no. 5, pp. 540–546, 2015.

[23] D. A. Hill, "Boundary fields in reverberation chambers," *IEEE Trans. Electromagn. Compat.*, vol. 47, no. 2, pp. 281–290, May 2005.

[24] J. B. Coder, J. M. Ladbury, C. L. Holloway, and K. A. Remley, "Examining the true effectiveness of loading a reverberation chamber: How to get your chamber consistently loaded," in *Proc. IEEE Int. Electromagn. Compat. Symp. Dig.*, Ft. Lauderdale, FL, USA, 2010, pp. 530–535.

[25] W. T. C. Burger, K. A. Remley, C. L. Holloway, and J. M. Ladbury, "Proximity and antenna orientation effects for large-form-factor devices in a reverberation chamber," in *Proc. IEEE Int. Electromagn. Compat. Symp. Dig.*, Aug. 5–9, 2013, pp. 671–676.

[26] C. L. Holloway, D. A. Hill, J. M. Ladbury, P. F. Wilson, G. Koepke, and J. Coder, "On the use of reverberation chambers to simulate a Rician radio environment for the testing of wireless devices," *IEEE Trans. Antennas Propag.*, vol. 54, no. 11, pp. 3167–3177, Nov. 2006.

[27] X. Chen, P.-S. Kildal, and S.-H. Lai, "Estimation of average Rician K-Factor and average mode bandwidth in loaded reverberation chamber," *IEEE Antennas Wireless Propag. Lett.*, vol. 10, pp. 1437–1440, 2011.

[28] K. A. Remley, R. J. Pirkl, H. A. Shah, and C.-M. Wang, "Uncertainty from choice of mode-stirring technique in reverberation-chamber measurements," *IEEE Trans. Electromagn. Compat.*, vol. 55, no. 6, pp. 1022–1030, Dec. 2013.

[29] J.G. Kostas and B. Boverie, "Statistical model for a mode-stirred chamber," *IEEE Trans. Electromagn. Compat.*, vol. 33, no. 4, pp. 366–370, Nov. 1991.

[30] K. Madsen, P. Hallbjörner, and C. Orlenius, "Models for the number of independent samples in reverberation chamber measurements with mechanical, frequency, and combined stirring," *IEEE Antennas Wireless Propag. Lett.*, vol. 3, no. 1, pp. 48–51, Dec. 2004.

[31] C. Lemoine, P. Besnier, and M. Drissi, "Estimating the effective sample size to select independent measurements in a reverberation chamber," *IEEE Trans. Electromagn. Compat.*, vol. 50, no. 2, pp. 227–236, May 2008.

[32] R. J. Pirkl, K. A. Remley, and C. Lötbäck Patané, "Reverberation chamber measurement correlation," *IEEE Trans. Electromagn. Compat.*, vol. 54, no. 3, pp. 533–545, Jun. 2012.

[33] X. Chen, "Experimental investigation of the number of independent samples and the measurement uncertainty in a reverberation chamber," *IEEE Trans. Electromagn. Compat.*, vol. 55, no. 5, pp. 816–824, Oct. 2013.

[34] X. Chen, P.-S. Kildal, C. Orlenius, and J. Carlsson, "Channel sounding of loaded reverberation chamber for over-the-air testing of wireless devices—Coherence bandwidth versus average mode bandwidth and delay spread," *IEEE Antennas Wireless Propag. Lett.*, vol. 8, pp. 678–681, 2009.

[35] *NIST Engineering Statistics Handbook* [Online]. Available: http://www.itl.nist.gov/div898/handbook/eda/section3/eda35c.htm

[36] E. Genender, C. L. Holloway, K. A. Remley, J. M. Ladbury, G. Koepke, and H. Garbe, "Simulating the multipath channel with a reverberation chamber: Application to bit error rate measurements," *IEEE Trans. Electromagn. Compat.*, vol. 52, no. 4, pp. 766–777, Nov. 2010.

[37] D. W. Matolak, K. A. Remley, C. L. Holloway, and C. Gentile, "Outdoor-to-indoor channel dispersion and power-delay profile models for the 700 MHz and 4.9 GHz bands," *IEEE Antennas Wireless Propag. Lett.*, vol. 15, pp. 441–443, 2016 [Online]. Available: http://dx.doi.org/10.1109/LAWP.2015.2451516

[38] K. A. Remley, W. F. Young, and J. Healy, "Analysis of radio-propagation environments to support standards development for RF-based electronic safety equipment," *NIST Technical Note 1559*, Mar. 2012.

Kate A. Remley (S'92–M'99–SM'06–F'13) was born in Ann Arbor, MI, USA. She received the Ph.D. degree in electrical and computer engineering from Oregon State University, Corvallis, OR, USA, in 1999.

From 1983 to 1992, she was a Broadcast Engineer in Eugene, OR, serving as Chief Engineer of an AM/FM broadcast station from 1989 to 1991. In 1999, she joined the RF Technology Division of the National Institute of Standards and Technology (NIST), Boulder, CO, USA, as an Electronics Engineer. She is currently the Leader of the Metrology for Wireless Systems Group at NIST, where her research activities include development of calibrated measurements for microwave and millimeter-wave wireless systems, characterizing the link between nonlinear circuits and system performance, and developing standardized test methods for RF equipment used by the public-safety community.

Dr. Remley was the recipient of the Department of Commerce Bronze and Silver Medals, an ARFTG Best Paper Award, and is a member of the Oregon State University Academy of Distinguished Engineers. She was the Chair of the MTT-11 Technical Committee on Microwave Measurements from 2008 to 2010 and the Editor-in-Chief of IEEE MICROWAVE MAGAZINE from 2009 to 2011, and is the Chair of the MTT Fellow Committee. She is a Distinguished Lecturer for the IEEE Electromagnetic Compatibility Society (2016–2018).

Jos Dortmans was born in Helmond, The Netherlands. He received the B.Sc. degree in electrical engineering from the Eindhoven University of Technology, Eindhoven, The Netherlands, in 2015, where he is currently working toward the M.Sc. degree in electrical engineering.

In 2015, he was a Guest Researcher at with the Electromagnetics Division, National Institute of Standards and Technology, Boulder, CO, USA. His current research interests include wireless communications and high-frequency measurements.

Catherine Weldon was born in Boulder, CO, USA, in 1993. She is currently working toward the B.Sc. degree in operations research and information engineering from Cornell University, Ithaca, NY, USA.

She was with the National Institute of Standards and Technology, Boulder, as a Guest Researcher during the summer of 2015. Her research interests include optimization methods and statistical modeling.

Robert D. Horansky (M'15) received the B.A. degree in chemistry and the Ph.D. degree in physics from the University of Colorado, Boulder, CO, USA, in 1999 and 2005, respectively. His thesis work focused on low-noise dielectric measurements on novel materials.

Since 2005, he has been with the National Institute of Standards and Technology (NIST), Gaithersburg, MD, USA, where he started out developing the highest resolving power energy dispersive sensor to date. He then went on to develop metrology techniques for single photon sensors in nuclear radiation and optical power measurements. In 2015, he joined the Metrology for Wireless Systems Group in the Communication Technology Laboratory, NIST developing calibrations and traceability for millimeter-wave wireless systems and reverberation-chamber measurements for cellular applications. He is the Secretary of the IEEE P1765 Standards Working Group on uncertainty for EVM and other wireless metrics.

Thomas B. Meurs (S'15) received the B.Sc. degree in electrical engineering from the Eindhoven University of Technology, Eindhoven, The Netherlands, in 2015, where he is currently working toward the M.Sc. degree in electrical engineering.

From 2015 to 2016, he was a Guest Researcher with the National Institute of Standards and Technology, Boulder, CO, USA. His research interests include the development of wireless communication and electromagnetic field applications in reverberation chambers, engineering toward healthcare solutions and electromagnetic compatibility.

Chih-Ming Wang received the Ph.D. degree in statistics from Colorado State University, Fort Collins, CO, USA, in 1978.

Since 1988, he has been with the Statistical Engineering Division, National Institute of Standards and Technology, Boulder, CO, USA. He has published more than 90 journal articles. His research interests include statistical metrology and the application of statistical methods to physical sciences.

Dr. Wang is a fellow of the American Statistical Association (ASA). He is the recipient of the Department of Commerce Silver Medal, Bronze Medal, the NIST Allen V. Astin Measurement Science Award, and several awards from ASA.

Dylan F. Williams (M'80–SM'90–F'02) received the Ph.D. degree in electrical engineering from the University of California, Berkeley, CA, USA, in 1986.

He joined the Electromagnetic Fields Division of the National Institute of Standards and Technology in 1989 where he develops electrical waveform and microwave metrology. He has published more than 100 technical papers.

Dr. Williams is the recipient of the Department of Commerce Bronze and Silver Medals, the Astin Measurement Science Award, two Electrical Engineering Laboratory's Outstanding Paper Awards, three Automatic RF Techniques Group (ARFTG) Best Paper Awards, the ARFTG Automated Measurements Technology Award, the IEEE Morris E. Leeds Award, the European Microwave Prize, and the 2013 IEEE Joseph F. Keithley Award. He also served as Editor of the IEEE TRANSACTIONS ON MICROWAVE THEORY AND TECHNIQUES from 2006 to 2010 and as the Executive Editor of the IEEE TRANSACTIONS ON TERAHERTZ SCIENCE AND TECHNOLOGY. He is currently the President Elect of the Microwave Theory and Techniques Society.

Christopher L. Holloway (S'86–M'92–SM'04–F'10) received the B.S. degree from the University of Tennessee at Chattanooga, TN, USA, in 1986, and the M.S. and Ph.D. degrees from the University of Colorado at Boulder, CO, USA, in 1988 and 1992, respectively, both in electrical engineering.

During 1992, he was a Research Scientist with Electro Magnetic Applications, Inc., Lakewood, CO, USA. His responsibilities included theoretical analysis and finite-difference time-domain modeling of various electromagnetic problems. From the fall of 1992 to 1994, he was with the National Center for Atmospheric Research (NCAR) in Boulder, CO. While at NCAR his duties included wave propagation modeling, signal processing studies, and radar systems design. From 1994 to 2000, he was with the Institute for Telecommunication Sciences (ITS) in the U.S. Department of Commerce in Boulder, CO, where he was involved in wave propagation studies. Since 2000, he has been with the National Institute of Standards and Technology (NIST), Boulder, CO, where he is involved in electromagnetic theory. He is also on the Graduate Faculty at the University of Colorado at Boulder. His research interests include electromagnetic field theory, wave propagation, guided wave structures, remote sensing, numerical methods, metamaterials, measurement techniques, EMC/EMI issues, and atom-based metrology.

Dr. Holloway is a member of URSI Commissions A, B, and E. He is currently serving as Chair for US Commission A of the International Union of Radio Science and is an Associate Editor for the IEEE TRANSACTIONS ON ELECTROMAGNETIC COMPATIBILITY. He was the Chair for the Technical Committee on Computational Electromagnetics (TC-9) of the IEEE Electromagnetic Compatibility Society from 2000 to 2005, served as Co-Chair for the Technical Committee on Nano-Technology and Advanced Materials (TC-11) of the IEEE EMC Society from 2006 to 2011, and served as an IEEE Distinguished Lecturer for the EMC Society from 2004 to 2006.

Perry F. Wilson (S'78–M'82–SM'93–F'05) received the Ph.D. degree in electrical engineering from the University of Colorado, Boulder, CO, USA, in 1983.

He currently leads the RF Fields Group in the RF Technology Division of the National Institute of Standards and Technology, Boulder, CO. His research has focused on the application of electromagnetic theory to problems in electromagnetic compatibility and RF field metrology.

Dr. Wilson is a member of US IEC TC77B TAG, past Editor-in-Chief of the IEEE EMC Transactions, a recipient of a 2010 IEEE EMC Society Technical Achievement Award, a recipient of the 2002 IEEE EMC Transactions Best Paper Award, and a recipient of a 2007 US Department of Commerce Gold Medal.